Organic-inorganic solar cell based on ZnO nanorod arrays

M. SIMA[*], E. VASILE[a], M. SIMA

National Institute of Materials Physics, 105bis Atomistilor Street, 077125 Magurele, Romania
[a]University "Politehnica"of Bucharest, Faculty of Applied Chemistry and Material Science, Department of Oxide Materials and Nanomaterials, No. 1-7 Gh. Polizu Street, 011061 Bucharest, Romania

In this study, we communicate an investigation on perovskite solar cell based on ZnO nanorod array and spiro OMeTAD film as electron and hole selective contacts. It was found that large thickness or small electrical conduction of the Li doped spiro OMeTAD layer and recombination processes at the interfaces contributed to the reduced efficiency of the solar cell.

1. Introduction

Getting cheap and clean energy from an abundant source is the goal of many researches that are ongoing today. Solar energy is today the most abundant energy resource used on Earth. The energy provided by the sun in a year is 100 times the energy of all known fossil fuel reserves. Therefore it is now seeking making cheap devices to more efficiently convert sunlight into electricity. Organic-inorganic hybrid solar cells like dye-sensitized solar cells (DSC) experienced significant developments in the last two decades [1]. However, they have not reached yet conversion efficiency large enough to compete on the energy market. A newcomer in the field of photovoltaics obtained from processing of organic solvent solutions is a solar cell with organic-inorganic perovskite ($CH_3NH_3PbX_3$, where X can be I, Cl, Br or their combination), a semiconductor with a perovskite structure containing Pb^{2+} ions, methylammonium ($CH_3NH_3^+$) and halide ions [2-9]. Standard perovskite solar cell structure contains a glass/FTO (fluorine-doped tin oxide) substrate covered with a compact layer of a wide band semiconductor (usually TiO_2). Over that is deposited a mesoporous scaffold from the same semiconductor which is in a close contact with a perovskite ($CH_3NH_3PbI_3$) film. Perovskite film which can work effectively as both absorber and an electron transporter is covered with a Li doped spiro OMeTAD film (hole transporter). A metallic contact (Au or Ag) is deposited on the spiro OMeTAD film. The presence of the compact layer of wide band semiconductor in the structure of the solar cell is to prevent the recombination of electrons in FTO with the holes in spiro OMeTAD.

ZnO is a possible alternative to TiO_2 in the perovskite solar cell structure. ZnO is a wide bandgap semiconductor with electron affinity similar to TiO_2. In addition, ZnO is known to have an electron mobility that is substantially higher than that of TiO_2 [10].

In our study we aimed to prepare zinc oxide nanorods that with perovskite layer to replace the photoelectrode based on TiO_2 from standard structure of the perovskite solar cell.

2. Experimental

ZnO nanorods were deposited on FTO substrate (with sheet resistance of 15ohm/square and its transmission > 80% from 400 to 700nm) during chemical processes from the solutions 1 and 2 from the Table 1. The substrate was thoroughly cleaned in an ultrasonic bath with isopropanol for 15 min prior to use. In order to prepare a seed layer on FTO substrate, the solution 1 was spincoated on the FTO substrate at a spinning rate of 2000 rpm for 20s, which was followed by annealing at 150^0C for 15min [11,12]. This procedure was repeated 3 times, and finally the seed layer was annealed at 350^0C for 15 min. The growth of ZnO nanorod arrays was achieved from the solution 2. The ZnO nanorod arrays were prepared by immersion of the seed layer deposited on FTO substrate for 60 and 180 min, respectively in the solution 2 at 90^0C. The prepared ZnO nanorod arrays were rinsed with distilled water and were annealed at 450^0C for 30 min. The perovskite solar cell was fabricated by deposition of perovskite film on the ZnO nanorod array in two step [4] and of Li doped spiro OMeTAD film. The solution 3 (Table 1) was dropped on the ZnO nanorods and the substrate was spin coated at 3000 rpm for 20s [13]. After the sample was dried at 100^0C for 10 min it was immersed into the solution 4 for 10 min. The obtained perovskite film was washed in 2-propanol and then was dried at 100^0C for 10 min. Over that it was deposited by spin coating (3000 rpm, 30s) a Li doped spiro OMeTAD film from the solution 5. Finally, a micrometric gold foil used as back contact was deposited by pressing on spiro OMeTAD film. The microstructures of the deposits were imaged by field emission scanning

electron microscopy (FESEM), using a FEY Quanta Inspect scanning electron microscope. X-ray diffraction (XRD) analyses were performed on a Bruker D8 Advance type X-ray diffractometer, in focusing geometry, equipped with copper target X-ray tube and LynxEye one-dimensional detector. The parameters of the solar cell were determined from I-V measurements carried out under standard illumination conditions using an AM1.5 solar simulator (L.O.T.-Oriel GmbH & Co.KG, Model LS0306 with a 300W Xe-Arc lamp and an AM1.5-Global filter (LSZ189) with the specification: 1sun at 18cm working distance). Photocurrent-voltage (I-V) measurements were

performed using an Autolab PGSTAT 30 Potentiostat/Galvanostat (Eco Chemie).
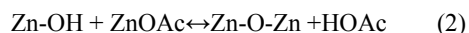
The Autolab PGSTAT 30 potentiostat with Frequency response analysis software, version 4.9 was used to conduct the electrochemical impedance spectroscopy (EIS) study, in order to determine the transport performance of the solar cell. The electrochemical impedance spectra were obtained at a bias of open-circuit voltage in 10^{-1} Hz $\leq$ f $\leq 10^5$ Hz frequency range with ac voltage amplitude of ± 10 mV, under 100mWcm^{-2} illumination.

Table 1

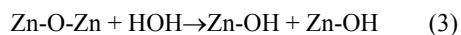| Solution	Composition
1	5mM Zn(CH$_3$COO)$_2$ x 2H$_2$O solution in ethanol
2	35mM Zn(NO$_3$)$_2$ + 35mM hexamethylenetetramine (C$_6$H$_{12}$N$_4$), aqueous solution
3	1M PbI$_2$ solution in N,N dimethylformamide (DMF), at 70^{0}C
4	0.063M CH$_3$NH$_3$I in anhydrous 2-propanol
5	0.170M 2,2',7,7'-tetrakis-(N,N-di-p-methoxyphenyl-amine)-9,9'-spirobifluorene (spiro-MeOTAD), 0.064 M bis(trifluoromethane)sulfonimide lithium salt (LiTFSI) and 0.198 M 4-tert-butylpyridine (TBP) in the mixed solvent of chlorobenzene and acetonitrile (chlorobenzene : acetonitrile=1 : 0.1 v/v).

3. Results and discussion

ZnO nanorod arrays have been prepared in a chemical process in aqueous solution with Zn(NO$_3$)$_2$ and C$_6$H$_{12}$N$_4$ as precursors. ZnO nanorods have been grown on ZnO seeded FTO surface. ZnO seed dots were prepared by the sol-gel technique using solution 1, Table 1. After the dissolution of zinc acetate dihydrate (Zn-OAc 2H$_2$O) in ethanol, zinc oxide can be formed by hydrolysis (1) and condensing (2) of the dissolved species [14]:

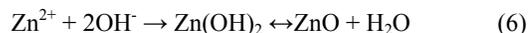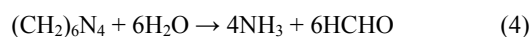$$Zn\text{-}OAc + HOH \leftrightarrow Zn\text{-}OH + HOAc \qquad (1)$$

$$Zn\text{-}OH + ZnOAc \leftrightarrow Zn\text{-}O\text{-}Zn + HOAc \qquad (2)$$

The process of hydrolysis of ZnO is equivalent to the dissolution of the ZnO.

$$Zn\text{-}O\text{-}Zn + HOH \rightarrow Zn\text{-}OH + Zn\text{-}OH \qquad (3)$$

The dissolved species were denoted as Zn-OAc in order to highlight the complexation of Zn^{2+} by acetate. After the process of condensation (2) and taking into account possible complexing of zinc with acetate it may form zinc-oxo-acetate oligomers. Progressive condensation of these oligomers will lead to the formation of colloids or precipitates [15].

Hexamethylenetetramine molecules act like a weak base which hydrolyzes slowly in the hot aqueous solution and, as a result, increases the pH of the solution and induces ZnO formation. It is important that the increase of the pH to go slow, otherwise Zn^{2+} ions will be quickly precipitated and their contribution to the growth of the nanorods will be reduced.

The chemical reactions which take place in the solution 2 from Table 1 at 90^{0}C are expressed by the following equations [16]:

$$(CH_2)_6N_4 + 6H_2O \rightarrow 4NH_3 + 6HCHO \qquad (4)$$

$$NH_3 + H_2O \rightarrow NH_4^+ + OH^- \qquad (5)$$

$$Zn^{2+} + 2OH^- \rightarrow Zn(OH)_2 \leftrightarrow ZnO + H_2O \qquad (6)$$

ZnO nanorod grown in this solution for one hour have diameters of about 140 nm and lengths up to 200 nm (Fig. 1) and those grown for 3 hours are longer (~ 500nm) but the tip diameter is less than 140nm (Fig. 2). We notice their high density that allows a good covering of the FTO substrate.

Over ZnO nanostructure from Fig. 2 was deposited a layer of perovskite by a method in two steps: deposition from the solution 3 of a layer of lead iodide which is then reacted on FTO substrate with methylammonium iodide in the solution 4.
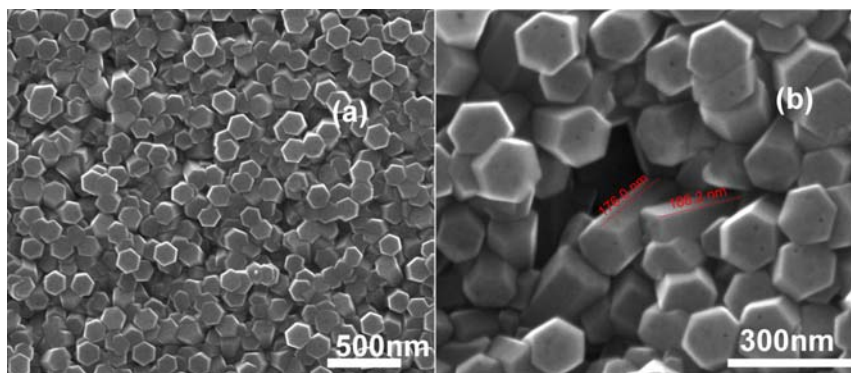
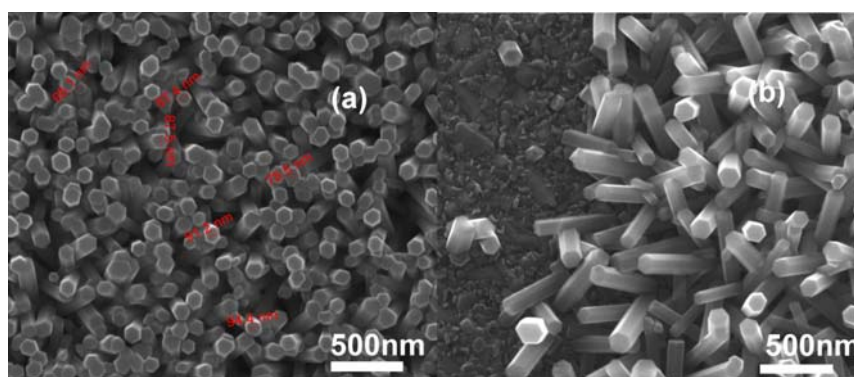*Fig.1. SEM images of the ZnO nanorod arrays prepared in the solution 2 from the Table 1 for 60 min.*

Fig.2. The morphology of the ZnO nanorod array prepared in the solution 2 from the Table 1 for 180 min.
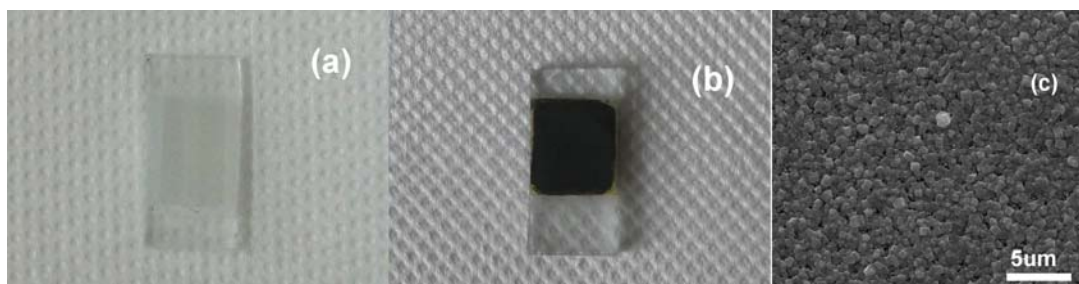

Fig.3. Photo images of the ZnO nanorod array (a) and of the perovskite film deposited on ZnO nanorod array (b); SEM image of the perovskite film deposited on ZnO nanorod array (c)

In the Fig. 3 are presented the photo images of the ZnO nanorod array and of the perovskite film deposited on ZnO nanorod array along with SEM image of the perovskite film deposited on ZnO nanorod array. SEM image (Fig. 3c) shows that perovskite layer is deposited especially on the tips of ZnO and covers partially ZnO nanorod array.

The X-ray diffraction pattern of the perovskite film deposited on ZnO nanorod array is shown in the Fig.4a. Relative intensities of ZnO diffraction peaks indicate that there is anisotropy in the distribution of crystallographic directions. In comparison with standard powder diffraction data [17] where the main diffraction peak corresponds to the crystalline planes family of Miller indices (101), it was found that the relative intensity of (002) peak is stronger compared to the others. This reflects that ZnO nanorods have a polycrystalline structure with preferred orientation in the direction [002]. The XRD pattern of the perovskite film (Fig. 4a and b) shows the presence of the PbI_2 peaks, revealing incomplete reaction between PbI_2 layer and methylammonium iodide in the solution 4.
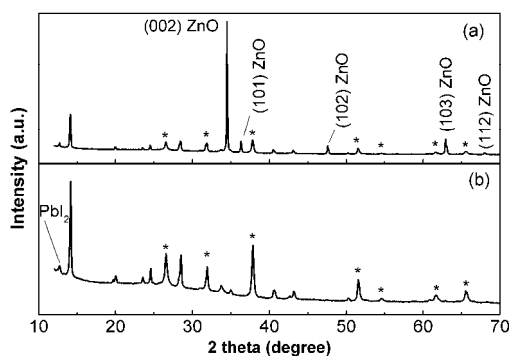
Fig.4. XRD patterns of the ZnO nanorod array covered with perovskite film (a) and of the perovskite film (b) deposited on FTO substrate (*).

IV characteristic of the solar cell measured under AM 1.5 illumination (100 mWcm^{-2}) is shown in the Fig 5a. Short-circuit current and the open circuit voltage were 2.2 mAcm^{-2} and 0.57V, respectively. Solar cell efficiency was 0.28%.

A further evaluation was performed by measuring impedance spectra of the solar cell.

These measurements are useful when the experimental data are fitted to representative equivalent circuit. The electrochemical impedance spectra were fitted using the Zview software by means of the equivalent circuits shown in Fig.5b.
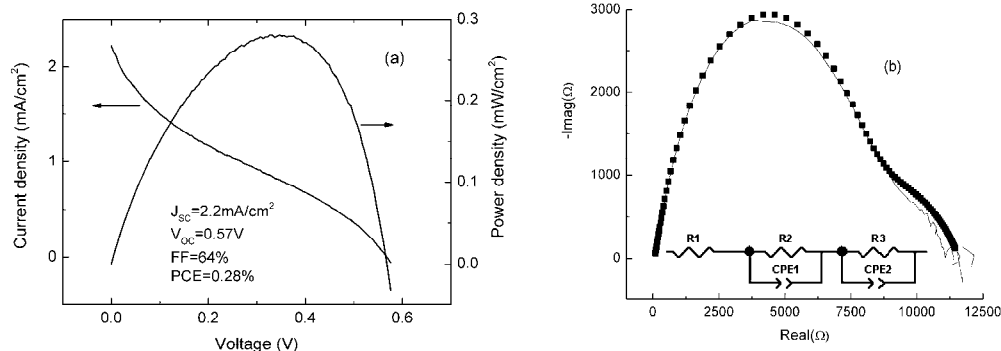

Fig.5. Evaluating of perovskite solar cell properties under AM 1.5 illumination: a) current density-voltage curve and b) Nyquist representation of the impedance spectrum of the solar cell and the circuit used to fit the measured data.

Impedance spectroscopy measurements (Fig.5b) were performed at open circuit voltage (0.57V), with solar cell under illumination AM 1.5. Nyquist representation of the solar cell shows two distinct RC arcs. The equivalent circuit of the cell includes: series resistance R_1 (the resistance of the FTO and the resistance of the contacts in the external circuit), and two RC circuits in series. To improve the quality of the fitting and considering the irregular nature of ZnO electrode there were used constant phase elements (CPE) instead of ideal capacitors. R_2-CPE_1 circuit is used to fit the impedance due to selective contacts (in our case, ZnO nanorod array and spiro OMeTAD film) and interfaces of these contacts with perovskite film. This impedance is responsible for the characteristics appearing at high frequencies in Nyquist representation [18]. CPE_1 is the capacity at the interface ZnO/perovskite.

R_3-CPE_2 is used to fit circuit impedance data at low frequencies. Resistance R_3 and capacitance CPE_2 are associated with recombination resistance and chemical capacitance, respectively, of the system [19]. The recombination processes mainly occur at interfaces. Their rate is inversely proportional to the recombination resistance, R_3 in our case. Chemical capacitance CPE_2 reveals the accumulation of charge carriers in perovskite

film. The parameter values obtained from the fitting with the equivalent circuit shown in Fig.5b are the following: R_1=0.5Ωcm^2, R_2=41Ωcm^2, R_3=75Ωcm^2, CPE_1=4x10^{-3} Fcm^{-2} si CPE_2=1.1x10^{-5}Fcm^{-2}.

Series resistance (R_1 in our case) is small for the samples containing hole-selective contact according to the literature [20]. Relative high value of the fill factor (FF) is in accordance with the value of this series resistance. On the other hand, resistance R_2 is dominated by hole-selective contact resistance when it is spiro OMeTAD film. In our case, the value of R_2 is about 2.5 times larger than corresponding values from literature [20], indicating a large thickness or a small electrical conduction of this layer. The obtained value R_3 is small compared to that from literature [18] which indicates a significant presence of the recombination processes at the interfaces.

4. Conclusions

We prepared by a chemical method ZnO nanorod arrays whose morphological and structural properties were studied. Also, we have fabricated a perovskite solar cell based on ZnO nanorod array and perovskite film. The manufactured solar cell efficiency is yet low. Impedance

spectroscopy study showed that the hole-selective contact (spiro OMeTAD) introduced a high resistance due to its large thickness or a small electrical conduction. It was also found a significant presence of the recombination processes.

References

[1] A. Yella, H.-W. Lee, H. N. Tsao, C. Yi, A.K. Chandiran, M.K. Nazeeruddin, E.W.-G. Diau, C.-Y. Yeh, S.M. Zakeeruddin, M. Gratzel, Science **334**, 629 (2011).

[2] A. Kojima, K. Teshima, Y. Shirai, T. Miyasaka, J. Am. Chem. Soc. **131**, 6050 (2009).

[3] H-S. Kim, C-R. Lee, J.-H. Im, K.-B. Lee, T. Moehl, A. Marchioro, S.-J. Moon, R. H.-Baker, J.-H. Yum, J. E. Moser, M. Gratzel, N.-G. Park, Sci. Rep. **2**, 591 (2012).

[4] J. Burschka, N. Pellet, S.-J. Moon, R. Humphry-Baker, P. Gao, M.K. Nazeeruddin, M. Gratzel, Nature **499,** 316 (2013).

[5] M. M. Lee, J.Teuscher, T. Miyasaka, T. N. Murakami, H. J. Snaith, Science **338,** 643 (2012).

[6] M. Liu, M. B. Johnston, H. J. Snaith, Nature **501**, 395 (2013).

[7] D.Y. Liu, T.L. Kelly, Nat. Photonics **8**, 133 (2014) .

[8] T.C. Sum, N. Mathews, Energy Environ. Sci. **7**, 2518 (2014) .

[9] N. J. Jeon,. J. H. Noh, W. S. Yang, Y. C. Kim, S. Ryu, J. Seo, S. I. Seok, Nature **517,** 476 (2015).

[10] Q. Zhang, C.S. Dandeneau, X. Zhou, G. Cao, Adv. Mater. **21**, 4087 (2009).

[11] L. E. Greene, Law, M.; J. Goldberger, F. Kim, J. C. Johnson, Y. Zhang, R. J. Saykally, P. Yang, Angew. Chem., Int. Ed. **42**, 3031 (2003).

[12] L. E. Greene, M. Law, D.H. Tan, M. Montano, J. Goldberger, G. Somorjai, P. Yang, Nano Lett. **5**, 1231 (2005).

[13] D-Y. Son, J-H. Im, H-S. Kim, N-G. Park, J. Phys. Chem. C **118**, 16567 (2014).

[14] E.A. Meulenkamp, J. Phys. Chem. B **102**, 5566 (1998).

[15] L. Zinaidi, Materials Science and Engineering B **174**, 18 (2010).

[16] X-D. Gao, X.-M. Li, W.-D. Yu, L. Li, J-J. Qiu, Appl. Surf. Sci. **253**, 4060 (2007).

[17] E.H. Kisi, M.M. Elcombe, Acta Crystallogr., Sec. C, **45**, 1967 (1989), Pattern No.79-2205.

[18] Y.Xu, J. Shi, S. Lv, L. Zhu, J. Dong, H. Wu, Y. Xiao, Y. Luo, S. Wang, D. Li, X. Li, Q. Meng, ACS, Appl.Mater. Interfaces **6**, 5651 (2014).

[19] I. Mora-Seró, J. Bisquert, F. Fabregat-Santiago, G. Garcia-Belmonte, K. Zoppi, D.Y., Y. Proskuryakov, I. Oja, A. Belaidi, T. Dittrich, R. Tena-Zaera, A. Katty, C. Lévy-Clement, V. Barrioz, S. J. C. Irvine, Nano Lett. **6**, 640 (2006).

[20] E.J. Juarez-Perez, M.Wuβler, F. Fabregat-Santiago, K. Lakus-Wollny, E.Mankel, T.Mayer, W. Jaegermann, I. Mora-Seró, J. Phys. Chem. Lett. **5**, 680 (2014).

_____
*Corresponding author at: msima@infim.ro